Mesoporous Silica Modified Luminescent Gd_2O_3:Eu Nanoparticles: Physicochemical and Luminescence Properties

Ali Aldalbahi[*1,2], Mostafizur Rahaman[2], Anees A. Ansari[*1]

[1]King Abdullah Institute for Nanotechnology, King Saud University, Riyadh-11451, Saudi Arabia

[2]Department of Chemistry, College of Sciences, King Saud University, Riyadh-11451

Abstract

Highly colloidal Eu-doped Gd_2O_3 nanoparticles(core-NPs) were synthesized by thermal decomposition via weak base at low temperature (150^{o}C), subsequently, silica layers were deposited to increased colloidal stability, solubility, biocompatibility and no-toxicity at the environmental condition. XRD results indicate the highly purified, crystalline, single phase cubic phase Gd_2O_3 nanocrystals. TEM image shows the mesoporous thick silica layer was effectively coated over the core nanocrystals, which have irregular size with nearly spherical shape and a mean grain size is about 10-30 nm. Absorption spectra and zeta potential results in aqueous media revealed that solubility, colloidal stability, and biocompatibility character was enhanced from core to core-shell structure because of silica layer surface encapsulation. The samples demonstrate excellent photoluminescence properties (dominant emission $^5D_0 \rightarrow {}^7F_2$ transition in red region at 610 nm) indicated the advantage to use in optical bio-detection and bio-labeling etc. The photoluminescence intensity of the silica shell modified core/shell nanoparticles were suppressed relatively core-nanoparticles, it indicates the multi-photon relaxation pathways arising from the surface coated high vibrational energy molecules of the silanol groups. The core/nSiO_2/mSiO_2 nanocrystals display strong emission ($^5D_0 \rightarrow {}^7F_2$) transition along with excellent solubility and biocompatibility, which may find promising applications in photonic based biomedical applications.

Keyword: Gadolinium oxide, mesoporous, silica, biocompatible, zeta potential, luminescence properties

Phone No.:+966-11-4676838 Fax No.:+966-11-4670662

Corresponding author Email: aaldalbahi@ksu.edu.sa, aneesaansari@gmail.com

 doi:10.20944/preprints201809.0138.v1

1. Introduction

In recent years, luminescent rare-earth inorganic materials has aroused rapidly growing interest for fluorescent-based biomedical applications because of their unique optical properties, such as sharp absorption and emission lines invisible region, low phonon energy, good quantum yield, narrow bandwidth, large stocks shift, high photo-chemical & thermal stability excellent biocompatibility and non-toxicity[1-5]. These outstanding optical and photochemical properties make them promising candidates for their future applications in widespread bio-medical sciences. Amongst lanthanide nanomaterials, gadolinium oxide (Gd_2O_3) is an ideal host matrix for doping of luminescent ion due to their excellent photo-chemical & thermal stability and low vibrational energy [1-3,5-7]. Additionally, Gd_2O_3 is magnetically active and used in magnetic resonance imaging contrast agent [2-4,8]. Therefore, trivalent Eu substituted Gd_2O_3 is one of the most important red-emitting inorganic material, because of its significant emission and exciton in UV/Visible regions [3,4,7]. Many efforts have been directed for the synthesis of Gd_2O_3 materials various chemical routes have been applied such as polyol[9,10], sono-chemical[11], micro-emulsion [12], sol-gel chemical[13], microwave decomposition[14,15], thermal decomposition[16,17], hydrothermal/solvo-thermal[18-20], co-precipitation[21-23], and aqueous self-combustion process. Among them, low-temperature thermal decomposition process can be the most efficient and appropriate synthesis routs as it can yield high phase purity powder with excellent chemical homogeneity. So that, micro to nano-scale Gd_2O_3:Ln synthesis methods with different morphologies via wet chemical process are considered better for their molecular level proper mixing. Because molecular level homogeneous mixing offers the possibilities for controlling the chemical composition, obtaining better-quality homogeneity, single phase, and higher surface area powders. Instead of ammonia or sodium hydroxide based co-precipitation process, urea-based thermal decomposition method is considered better process [24-28]. Urea-based thermal decomposition process has an advantage, homogeneous precipitation generates fine small particles, which are relatively narrow size distribution with the large surface area and high porosity comparative to others. Additionally, it takes advantage of the exothermic, fast, and self-sustaining chemical reactions between lanthanide nitrates/chlorides and the weak base

Preprints (www.preprints.org) | NOT PEER-REVIEWED | Posted: 7 September 2018 doi:10.20944/preprints201809.0138.v1

(Urea) reducing agent. As a consequence, it is particularly highly suitable for the elaboration of uniform nano-crystalline particles of lanthanides with the high specific surface area and superfine dimensions.

In the present study, we illustrated the single step procedure for the synthesis of europium-doped gadolinium oxide nanoparticles (Core-NPs) via thermal decomposition process at low temperature with an average 10-30 nm, which were well monodispersed and shows high dispersibility in aqueous media. Consequently, the prepared core-NPs were covered through amorphous silica layer to improve their solubility, biocompatibility and toxicity character at environmental conditions. These core and silica surface modified core-shell NPs were fully characterized systematically via different physio-chemical techniques such as X-ray diffraction pattern(XRD), transmission electron microscopy (TEM), energy dispersive x-ray analysis(EDX), thermogravimetric analysis(TGA), zeta potential, Fourier transform infrared (FTIR), UV/Visible, excitation and emission spectroscopy to examine their crystallinity, phase purity, crystal structure, surface morphology, thermal durability, surface chemistry, solubility, biocompatibility optical absorption and photoluminescence properties. For biomedical applications, it is an urgent need to functionalized or cover the surface with active functional groups or organic ligands to enhance their aqueous solubility character, which can easily available to conjugation with bio-macromolecules as per requirement. For surface coating or functionalization, silica shell coating process is well accepted to grown over the surface of the luminescent core-nanoparticles by co-hydrolysis and poly-condensation with tetraethyl-orthosilicate (TEOS)[10,29,30]. The surface grew silanol (Si-OH) groups are easily available for conjugation or binding with organic bio-macromolecules and used as highly fluorescent, sensitive and reproducible biomedical applications. Additionally, the surface functionalized nanoparticles with the high surface area and mesoporosity allow for designing multifunctional systems for simultaneous drug delivery and cell imaging.

2. Experimental section

2.1. Materials

Gd_2O_3 (99.99%, BDH Chemicals, UK), Eu_2O_3 (99.99%, AlfaAesar, Germany), NH_4OH, NaOH, ethyl alcohol, urea, tetraethyl-orthosilicate (TEOS), N-

Preprints (www.preprints.org) | NOT PEER-REVIEWED | Posted: 7 September 2018 doi:10.20944/preprints201809.0138.v1

cetyltrimethylammonium bromide (CTAB) were used directly as-received without further purification. Gadolinium nitrate and europium nitrate were prepared by dissolving the corresponding metal oxides in the diluted nitric acid. Milli-Q (Millipore, Bradford, USA) water was used for synthesis and characterization of the samples.

2.2. Synthesis of Gd_2O_3:Eu (Core), Gd_2O_3:Eu@nSiO_2(Core/nSiO_2) and Gd_2O_3:Eu@ nSiO_2@mSiO_2 (core/nSiO_2/mSiO_2)nanoparticles

In a typical procedure for the synthesis of Gd_2O_3:Eu nanoparticles(core), 4.5 g gadolinium nitrate hexahydrate and 0.223 g europium nitrate hexahydrate were mixed together in a 100 ml dist. water and kept on a hot plate at 80 ^oC under constant mechanical stirring. Then an appropriate amount of urea dissolved in aqueous media was introduced into the vigorously stirred solution mixture. After that, the transparent solution mixture was transferred into round bottle flask and kept under a refluxed condition at 150 ^oC for 3-4 h. The obtained white precipitate was separated by centrifugation washed several times with distilled water and dried in an oven overnight. This dried sample was further calcinied at 750 ^oC under air condition. Stober sol-gel chemical method was followed for nanoporous silica (nSiO_2) surface coating as discussed in previous literature reports [10,29,30]. For mesoporous silica (mSiO_2) surface coating modified sol-gel method was applied. A solution containing100 mg Gd_2O_3:Eu@nSiO_2,100 mg CTAB and 50 mg NaOH were dissolved in 250 ml distilled water on a hot plate at 80 ^oC with constant mechanical stirring[31-35]. Afterward 1.0 ml TEOS was introduced slowly into the vigorously mechanical stirred solution. The mixed solution was allowed to co-hydrolysis and condensation for 2 hrs, to give a white precipitate. Occurred precipitate was separated by centrifugation, washed several times with water and dried in an oven to yield the mesoporous core-shell/Si nanoparticles.

2.4. Characterization

Powder X-ray diffraction pattern (PANalytical X'Pert, X-ray diffractometer) equipped with Ni filter Cu$K\alpha$ (λ = 1.5404Å) radiation was used for examining the phase purity and crystal structure of the samples. Field emission-transmission electron microscope (FE-TEM, JEM-2100F, JEOL, Japan) equipped with energy dispersive x-ray (EDX) analysis operating at an accelerating voltage 200kV was applied for morphology

Preprints (www.preprints.org) | NOT PEER-REVIEWED | Posted: 7 September 2018 doi:10.20944/preprints201809.0138.v1

inspection. Zeta potential was measured from zeta sizer (Brookhaven Instruments Corporation Holtsville, NY, USA). Thermal analysis was obtained from the thermogravimetric analyzer (Mettler Toledo, Analytical CH-8603 Schwarzenbach, Switzerland). FTIR spectra were measured from Vertex 80(Bruker, USA) infrared spectrometer with KBr pellet technique. Absorption spectra were recorded using by Cary 60 (Agilent Technologies, USA) UV-Vis spectrophotometer from 200-600 nm. Photoluminescence spectra were obtained from Fluorolog 3(Model: FL3-11, Horiba Jobin Yvon, USA) photoluminescence spectrophotometer.

3. Results and Discussion

X-ray diffraction pattern was allowed to determine the phase purity, crystal structure, and crystallinity of the as-prepared samples. Fig. 1 illustrate the XRD pattern of Gd_2O_3:Eu core, core/nSiO_2 and core/nSiO_2/mSiO_2 samples. All reflection peaks in all three diffractograms are well indexed to the JCPDS card No. 012-0797 resulted cubic Gd_2O_3 phase [3,4,6,36,37]. No impurity is detected over the entire XRD range indicated the Eu^{3+} ion is homogeneously distributed inside the crystal lattice and formation of single phase pure cubic Gd_2O_3 nanoparticles. The observed broadening in reflection peak width is related to the nanocrystalline size of the as-synthesized samples. An observed reduction in reflection peak intensity is implying the influence of amorphous silica surface coating over the luminescent core-NPs[38]. The most prominent diffraction peak observed at $2\theta = 28.79^{o}$ is used for calculating the average grain size of the NPs. The experimentally estimated crystalline size of the core, core/nSiO_2, and core/nSiO_2/mSiO_2 NPs are to be 10, 19, 35 nm, respectively.

Morphological structure of the as-synthesized core, core/nSiO_2 and core/nSiO_2/ mSiO_2 NPs was determined from TEM micrographs. TEM image in Fig.2a illustrate the highly aggregated, quasi-spherical shaped, well distributed, porous, crystalline nanoparticles with an average 10-30 nm. As seen in typical high-resolution TEM micrographs, spherical shaped nanoparticles have a large number of pores which are randomly arranged and distributed homogeneously throughout the entire particle. This high porosity of the luminescent nanoparticles is facilitating insolubility and high colloidal stability in an aqueous environment. We expected, that the existence of the little

Preprints (www.preprints.org) | NOT PEER-REVIEWED | Posted: 7 September 2018 doi:10.20944/preprints201809.0138.v1

amount of urea and surfactants enhanced the aggregation or clustering of the spherical shaped nanoparticles. The lattice fringes in individual nanoparticles are obvious as observed in high-resolution TEM image (Fig.2c), suggests the highly crystalline nature of the materials. The lattice planes are well separated and possessed a uniform lattice structure with the well-indexed lattice fringes d_{222}= 0.311Å, which is well consistent with the d-spacing value of (222) lattice planes of cubic phase Gd_2O_3 structure, this value is corroborated with the reported value for Gd_2O_3 NPs(Fig2c)[39-41]. As observed in Fig.2d&e a uniform, thick mesoporous silica layer possesses a wormhole-channel like structure with a thickness of 55 nm has been effectively grown over the surface of luminescent core-NPs. As seen in Fig.2d, after encapsulation of silica layer around the core NPs, the morphology of the core NPs is still maintained, it indicates that mesoporous silica layer has no side effect on the uniformity of the core NPs. The mesoporous silica shell is a contrast in color due to different electron penetrability between the core and an amorphous silica layer. The silica shell is light gray color and the core is dark black in color (Fig.2e). EDX analysis was performed to verify the doping constituents and silica surface coating surrounding the luminescent core-NPs. The EDX profile confirmed the existence of gadolinium (Gd), oxygen (O) and europium(Eu) in the core NPs, suggesting the Eu^{3+} ion is homogeneously distributed inside the Gd_2O_3 crystal lattice(Fig.2f&g). An additional peak of silica is observed in core/nSiO_2/mSiO_2 NPs at around 1.8 keV, indicate the successful silica coating around the core-NPs. The appearance of strong C and Cu peak in the spectra is belonging to the carbon coated copper grid. No other assigned peaks are detected in both EDX spectrums, it suggests the phase purity of the NPs.

The solubility character, colloidal stability and surface charge of the as-synthesized luminescent NPs were further verified from zeta potential. As illustrate in Fig.3 the zeta potential values of core and core/nSiO_2 NPs at physiological pH (pH = 7.0) are 22.8 and -14.2 mV, respectively (Fig.3a&b). Additionally, on increasing the pH values from 8 to 10 in aqueous solution the zeta potential values gradually decrease -13.9 and -19.9 mV, respectively (data not shown). Whereas, the zeta potential values for silica modified core/nSiO_2/mSiO_2 NPs at 8 and 10 pH are -39.5 and -34.2 mV, respectively (Fig.3c&d). Notably, the zeta potential value in core/nSiO_2/mSiO_2 NPs is greatly

Preprints (www.preprints.org) | NOT PEER-REVIEWED | Posted: 7 September 2018 doi:10.20944/preprints201809.0138.v1

decreased with respect to the core-NPs. It suggests the successful silica surface modification over the luminescent core-NPs[42-44]. It is fact that mesoporous silica having abundant surface hydroxyl groups and provides powerful claw for easily binding with hydroxyl groups or bio-macromolecules to form complexation[38,42,45]. These surface attached hydroxyl molecules or silanol(Si-OH) groups make a strong coordination bond between core/nSiO_2/mSiO_2 NPs and bio-macromolecules[38,42,46]. We expected that on increasing the pH value the concentration of hydroxyl ion is an increase, these free hydroxyl (OH^-) ions bind with positively charged silica modified core/nSiO_2/mSiO_2 NPs for neutralization and make a complex, resulting the zeta potential values are continuously decreasing [1,42,43]. These facts obviously confirm the solubility and excellent colloidal stability character across a broad range of pH values and further verified the surface charged over the core and surface functionalized core/nSiO_2/mSiO_2 NPs [38,42,46].

Thermal analysis was performed to analyze the surface adsorbed organic moieties and thermal stability of the as-synthesized NPs. The thermogram of core and core/nSiO_2 NPs nanoparticles demonstrate two-stage thermal decomposition. The first weight loss approximately 2.5% in core nanoparticles occurs between 50-330 ^oC, which seems to the removal of surface adsorbed residual water molecules and organic moieties (Fig.4). After that, in second stage approximately 3.5% weight loss is observed in between 330 to 800 ^oC, which corresponds to the combustion and elimination of surface capping oxygen species along with bulk oxygen species and formation of Gd_2O_3 nano-product. Whereas in the case of core/nSiO_2 NPs, initial weight loss is recorded below 200 ^oC it shows the removal of surface adsorbed residual water molecules. After that, a continuous greatest weight loss (~8%) is measured up to 800 ^oC, it implies to the burning and elimination of surface modified silica, in which silica is transforming into silicate agreeing well with TEM and EDX analysis[47].

The silica surface coating was further validated from FTIR spectra with the characteristic peaks of amorphous silica molecules. Compared with the infrared spectrum of Core sample, nSiO_2 and mSiO_2 coated samples have doublet high-intensity band located at 1097 cm^{-1} along with weak sharp intensity bands at 798 and 600 cm^{-1}, which

Preprints (www.preprints.org) | NOT PEER-REVIEWED | Posted: 7 September 2018 doi:10.20944/preprints201809.0138.v1

are originating from stretching and bending vibrational modes of Si-O-Si, Si-O and Si-OH surface modified amorphous silica (Fig.5) [48-53]. A diffused broad intensity band is observed in all three spectra located at 3425 cm^{-1} along with middle-intensity infrared band located at 1517 and 1405 cm^{-1} are ascribed to the stretching and bending vibrational modes of surface adsorbed residual water molecules[29,33,43,54]. These observations are supported well with the XRD, TEM, EDX and TGA analysis and previously published literature reports [9,42,43,51,52]. A sharp infrared absorption peak is observed at 549 cm^{-1} in all three spectra, which is attributed to the stretching vibration of M-O network [55]. Optical absorption spectra were performed to investigate the optical properties, solubility and colloidal stability character in an aqueous environment. Absorption spectra of core and core/nSiO_2 NPs were recorded in dist. water (Fig.6). The core/nSiO_2 NPs sample exhibits strong absorbance in the visible region, which is assigned to the $^8S_{7/2}\rightarrow{}^6I_j$ transition of Gd(III) ion and existence of the amorphous silica surrounding the core-NPs [29,32,45,56].

Photoluminescence measurement was performed to confirm the Eu(III) ion doping and amorphous silica surface modification around the core-NPs. Fig.7 illustrate the excitation spectra of core, core/nSiO_2 and core/nSiO_2/mSiO_2 NPs under monitoring 610 ($^5D_0\rightarrow{}^7F_2$) nm emission wavelength at room temperature. The excitation spectra consist of several sharp excitation electronic transitions assigned to $^7F_0\rightarrow{}^5H_{3,6}$(321), $^7F_0\rightarrow{}^5D_4$(362), $^7F_0\rightarrow{}^5G_3$(381), $^7F_0\rightarrow{}^5L_6$(394), $^7F_0\rightarrow{}^5D_3$(415), and $^7F_0\rightarrow{}^5D_2$(466), which are originating from 4*f*-4*f*-intra-configurationally transitions of Eu^{3+} ions[30,37,47,54,57-59]. Figure 8 demonstrates the emission spectra of core, core/nSiO_2 and core/nSiO_2/ mSiO_2 NPs upon excitation at 395 nm on room temperature. The obtained spectra displays characteristic emission transitions of Eu^{3+}ions at 464-474 ($^5D_2\rightarrow{}^7F_0$), 531-538 ($^5D_1\rightarrow{}^7F_1$), 578($^5D_1\rightarrow{}^7F_3$), 585-599 ($^5D_0\rightarrow{}^7F_1$), 605-631 ($^5D_0\rightarrow{}^7F_2$), 644-662 ($^5D_0\rightarrow{}^7F_3$) and 684-712 ($^5D_0\rightarrow{}^7F_4$) transitions, respectively[6,29,30,47,59,60]. Some weak intensity emission transitions located at 470 and 535 nm assigned to $^5D_2\rightarrow{}^7F_0$ and $^5D_1\rightarrow{}^7F_1$ transition of Eu^{3+} ion, it indicate the low vibrational energy of the Gd-O band[6,58]. Consequently, the multiphonon relaxation by gadolinium-oxygen vibration is not able to bridge the gaps between the higher energy levels of $^5D_2\rightarrow{}^7F_0$ & $^5D_1\rightarrow{}^7F_1$ transition and

Preprints (www.preprints.org) | NOT PEER-REVIEWED | Posted: 7 September 2018 doi:10.20944/preprints201809.0138.v1

the $^5D_0 \rightarrow {}^7F_J$ level of Eu(III) ion completely, resulting in the emission from these levels[59]. A prominent emission transition is observed in between 605-630 nm because of $^5D_0 \rightarrow {}^7F_2$ forced electric dipole transition and is hypersensitive to the environment[30,47,60]. The emission band observed at around 585-598 nm is assigned to magnetic dipole transition which is weak with respect to forced electric dipole transition [30,60]. It is fact that forced electric dipole transition ($^5D_0 \rightarrow {}^7F_2$) is sensitive to the surrounding chemical environment whereas magnetic dipole transition ($^5D_0 \rightarrow {}^7F_1$) is independent to the surrounding environment [30,47,60,61]. It is obvious from the emission spectra of all three samples the emission efficiency of hypersensitive transition or electric dipole transition is higher than their respective magnetic dipole transition, it suggests that the trivalent europium ions are in the C_2 site symmetry. We speculate that, in the cubic crystal structure of Gd_2O_3, Gd^{3+} have C_2 and S_6 symmetric site which are both octahedral coordination. In the C_2 site, four equal equatorial Gd-O and two apical Gd-O bonds have different bond distances. However, the S_6 site has equal bond distances (Gd-O) and inversion center [6,37,57-59,62]. In that case, if Eu(III) ions occupy the S_6 site symmetry of Gd^{3+} ions, the magnetic dipole transition will be obtained. In fact, the emission spectra simplify that most of the Eu^{3+} ions had C_2 symmetry as compared to the S_6 symmetry, resulting the predominant high emission intensity transition is achieved. It is interesting to note, that the ^7F_J energy levels of Eu^{3+} split into some components under crystal field effects caused by the surrounding ions. Under C_2 site symmetry, $^5D_0 \rightarrow {}^7F_1$ and $^5D_0 \rightarrow {}^7F_2$ are split in multiple times, it could be due to the completely lifted "$2J$+1" degeneracy of the ground state electronic configuration of Eu^{3+}. These results are in excellent consistent with the previous reports [3,6,30,37,57-59,62]. It is worth noticing that, the emission intensity is suppressed in core/nSiO_2 NPs, which is further greatly quenched after mesoporous silica surface coating over the core/nSiO_2 NPs. The reduction in emission and excitation intensity is related to the formation of interfacial high phonon energy surface quenching sites by the amorphous silica and organic moieties as supported by EDX, TGA, and FTIR analysis. These surface formed high vibrational energy quenching sites enhanced the nonradiative transition pathways and suppressed the photoluminescence efficiency of the NPs. These results are in excellent agreement with

Preprints (www.preprints.org) | NOT PEER-REVIEWED | Posted: 7 September 2018 doi:10.20944/preprints201809.0138.v1

the previously published reports [30,50,52,63-66]. Additionally, the luminescent intensity is also associated to the structural characteristics such as crystal field effect, that is closely related to the structure and its symmetry, oxygen vacancies which also act as a quenching center for photoluminescence[67]. It is fact that amorphous silica surface suppressed the luminescence efficiency, whereas enhanced the solubility, colloidal stability, biocompatibility and non-toxic nature of the luminescent materials regardless non-silica modified luminescent core-NPs[30,50,68-70].

4. Conclusion

In conclusion colloidal, mesoporous silica surface modified Gd_2O_3:Eu@nSiO_2@mSiO_2 nanoparticles were successfully synthesized by urea-based thermal decomposition process at low temperature, subsequently, amorphous silica layer was developed by sol-gel chemical routs. The obtained core nanoparticles are highly crystalline, irregular spherical size, rough surface with narrow size distribution. TEM images clearly revealed the successful mesoporous silica surface coating over the core nanoparticles. Absorption spectra demonstrate the high solubility and colloidal stability, which verified from zeta potential results. A remarkable enhancement in solubility, colloidal stability, and biocompatibility character was observed in silica surface modified core-shell/Si nanoparticles due to the surface anchored hydroxyl groups. FTIR spectral results proved the surface anchored silanol groups. The core nanoparticles revealed strong emission transition in the red region (612 nm) even after covering of amorphous silica layer. However, the emission intensity of silica layer cover nanoparticles was quenched relatively their uncoated counterpart because of multiphoton-relaxation pathways from high phonon energy hydroxyl groups. These high vibrational energy groups scattered the incident and emission light, resulting in suppressed the emission intensity of the nanomaterials. Whereas, these surface cover hydroxyl groups (Si-OH) enhanced the solubility, biocompatibility and non-toxic nature of the materials. Our finding illustrates the successful approach for the synthesis of very bright red phosphors for their use in broad photonic based biomedical applications like as optical bio-sensor/detection/labeling and bio-imaging etc.

Acknowledgment: The authors extend their appreciation to the Deanship of Scientific Research at King Saud University for funding this work through Research Group No. RG-1436-005.

References

1. Li, I.F.; Su, C.H.; Sheu, H.S.; Chiu, H.C.; Lo, Y.W.; Lin, W.T.; Chen, J.H.; Yeh, C.S. Gd2o(co3)(2)center dot h2o particles and the corresponding gd2o3: Synthesis and applications of magnetic resonance contrast agents and template particles for hollow spheres and hybrid composites. *Advanced Functional Materials* **2008**, *18*, 766-776.
2. Shao, Y.Z.; Tian, X.M.; Hu, W.Y.; Zhang, Y.Y.; Liu, H.; He, H.Q.; Shen, Y.Y.; Xie, F.K.; Li, L. The properties of gd2o3-assembled silica nanocomposite targeted nanoprobes and their application in mri. *Biomaterials* **2012**, *33*, 6438-6446.
3. Liu, Y.C.; Yang, P.P.; Wang, W.X.; Dong, H.X.; Lin, J. Fabrication and photoluminescence properties of hollow gd2o3:Ln (ln = eu3+, sm3+) spheres via a sacrificial template method. *Crystengcomm* **2010**, *12*, 3717-3723.
4. Tian, G.; Gu, Z.J.; Liu, X.X.; Zhou, L.J.; Yin, W.Y.; Yan, L.; Jin, S.; Ren, W.L.; Xing, G.M.; Li, S.J.*, et al.* Facile fabrication of rare-earth-doped gd2o3 hollow spheres with upconversion luminescence, magnetic resonance, and drug delivery properties. *J Phys Chem C* **2011**, *115*, 23790-23796.
5. Yang, G.X.; Lv, R.C.; Gai, S.L.; Dai, Y.L.; He, F.; Yang, P.P. Multifunctional sio2@gd2o3:Yb/tm hollow capsules: Controllable synthesis and drug release properties. *Inorganic Chemistry* **2014**, *53*, 10917-10927.
6. Raju, G.S.R.; Pavitra, E.; Yu, J.S. Facile template free synthesis of gd2o(co3)(2).H2o chrysanthemum-like nanoflowers and luminescence properties of corresponding gd2o3:Re3+ spheres. *Dalton T* **2013**, *42*, 11400-11410.
7. Shi, H.Z.; Li, L.; Zhang, L.Y.; Wang, T.T.; Wang, C.G.; Su, Z.M. Facile fabrication of hollow mesoporous eu3+-doped gd2o3 nanoparticles for dual-modal imaging and drug delivery. *Dyes and Pigments* **2015**, *123*, 8-15.
8. Huang, C.C.; Liu, T.Y.; Su, C.H.; Lo, Y.W.; Chen, J.H.; Yeh, C.S. Superparamagnetic hollow and paramagnetic porous gd2o3 particles. *Chem Mater* **2008**, *20*, 3840-3848.
9. Ansari, A.A.; Parchur, A.K.; Alam, M.; Azzeer, A. Effect of surface coating on optical properties of eu3+-doped camoo4 nanoparticles. *Spectrochim Acta A* **2014**, *131*, 30-36.
10. Ansari, A.A.; Parchur, A.K.; Alam, M.; Labis, J.; Azzeer, A. Influence of surface coating on structural and photoluminescent properties of camoo4:Pr nanoparticles. *Journal of Fluorescence* **2014**, *24*, 1253-1262.
11. Zhu, L.; Liu, X.M.; Liu, X.D.; Li, Q.; Li, J.Y.; Zhang, S.Y.; Meng, J.; Cao, X.Q. Facile sonochemical synthesis of cepo4 : Tb/lapo4 core/shell nanorods with highly improved photoluminescent properties. *Nanotechnology* **2006**, *17*, 4217-4222.
12. Chai, R.T.; Lian, H.Z.; Yang, P.A.P.; Fan, Y.; Hou, Z.Y.; Kang, X.J.; Lin, J. In situ preparation and luminescent properties of lapo4:Ce3+, tb3+ nanoparticles and transparent lapo4:Ce3+, tb3+/pmma nanocomposite. *J Colloid Interf Sci* **2009**, *336*, 46-50.
13. Grzyb, T.; Weclawiak, M.; Lis, S. Influence of nanocrystals size on the structural and luminescent properties of gdof:Eu3+. *Journal of Alloys and Compounds* **2012**, *539*, 82-89.

14. Ding, M.Y.; Lu, C.H.; Ni, Y.R.; Xu, Z.Z. Rapid microwave-assisted flux growth of pure beta-nayf4:Yb3+, ln(3+) (ln = er, tm, ho) microrods with multicolor upconversion luminescence. *Chemical Engineering Journal* **2014**, *241*, 477-484.
15. Mi, C.C.; Tian, Z.H.; Han, B.F.; Mao, C.B.; Xu, S.K. Microwave-assisted one-pot synthesis of water-soluble rare-earth doped fluoride luminescent nanoparticles with tunable colors. *Journal of Alloys and Compounds* **2012**, *525*, 154-158.
16. Liu, X.X.; Ni, Y.R.; Zhu, C.; Fang, L.; Kou, J.H.; Lu, C.H.; Xu, Z.Z. Controllable self-assembly of naref4 upconversion nanoparticles and their distinctive fluorescence properties. *Nanotechnology* **2016**, *27*.
17. Naccache, R.; Vetrone, F.; Mahalingam, V.; Cuccia, L.A.; Capobianco, J.A. Controlled synthesis and water dispersibility of hexagonal phase nagdf4:Ho3+/yb3+ nanoparticles. *Chem Mater* **2009**, *21*, 717-723.
18. Chaudhary, S.; Kumar, S.; Umar, A.; Singh, J.; Rawat, M.; Mehta, S.K. Europium-doped gadolinium oxide nanoparticles: A potential photoluminescencent probe for highly selective and sensitive detection of fe3+ and cr3+ ions. *Sensors and Actuators B-Chemical* **2017**, *243*, 579-588.
19. Chen, G.W.; Qi, W.C.; Li, Y.B.; Yang, C.S.; Zhao, X.P. Hydrothermal synthesis of y2o3:Eu3+ nanorods and its growth mechanism and luminescence properties. *Journal of Materials Science-Materials in Electronics* **2016**, *27*, 5628-5634.
20. Dhananjaya, N.; Nagabhushana, H.; Nagabhushana, B.M.; Rudraswamy, B.; Shivakumara, C.; Chakradhar, R.P.S. Hydrothermal synthesis, characterization and raman studies of eu3+ activated gd2o3 nanorods. *Physica B-Condensed Matter* **2011**, *406*, 1639-1644.
21. Marques, V.S.; Cavalcante, L.S.; Sczancoski, J.C.; Alcantara, A.F.P.; Orlandi, M.O.; Moraes, E.; Longo, E.; Varela, J.A.; Li, M.S.; Santos, M.R.M.C. Effect of different solvent ratios (water/ethylene glycol) on the growth process of camoo4 crystals and their optical properties. *Crystal Growth & Design* **2010**, *10*, 4752-4768.
22. Runowski, M.; Ekner-Grzyb, A.; Mrowczynska, L.; Balabhadra, S.; Grzyb, T.; Paczesny, J.; Zep, A.; Lis, S. Synthesis and organic surface modification of luminescent, lanthanide-doped core/shell nanomaterials (lnf(3)@sio2@nh2@organic acid) for potential bioapplications: Spectroscopic, structural, and in vitro cytotoxicity evaluation. *Langmuir* **2014**, *30*, 9533-9543.
23. Shete, P.B.; Patil, R.M.; Thorat, N.D.; Prasad, A.; Ningthoujam, R.S.; Ghosh, S.J.; Pawar, S.H. Magnetic chitosan nanocomposite for hyperthermia therapy application: Preparation, characterization and in vitro experiments. *Applied Surface Science* **2014**, *288*, 149-157.
24. Song, Y.H.; You, H.P.; Huang, Y.J.; Yang, M.; Zheng, Y.H.; Zhang, L.H.; Guo, N. Highly uniform and monodisperse gd2o2s:Ln(3+) (ln = eu, tb) submicrospheres: Solvothermal synthesis and luminescence properties. *Inorganic Chemistry* **2010**, *49*, 11499-11504.
25. Yang, J.; Quan, Z.W.; Kong, D.Y.; Liu, X.M.; Lin, J. Y2o3 : Eu3+ microspheres: Solvothermal synthesis and luminescence properties. *Crystal Growth & Design* **2007**, *7*, 730-735.
26. Zhang, C.M.; Cheng, Z.Y.; Yang, P.P.; Xu, Z.H.; Peng, C.; Li, G.G.; Lin, J. Architectures of strontium hydroxyapatite microspheres: Solvothermal synthesis and luminescence properties. *Langmuir* **2009**, *25*, 13591-13598.
27. Jia, G.; You, H.P.; Liu, K.; Zheng, Y.H.; Guo, N.; Zhang, H.J. Highly uniform gd2o3 hollow microspheres: Template-directed synthesis and luminescence properties. *Langmuir* **2010**, *26*, 5122-5128.

28. Jia, G.A.; You, H.P.; Song, Y.H.; Huang, Y.J.; Yang, M.; Zhang, H.J. Facile synthesis and luminescence of uniform y2o3 hollow spheres by a sacrificial template route. *Inorganic Chemistry* **2010**, *49*, 7721-7725.
29. Ansari, A.A.; Alam, M.; Labis, J.P.; Alrokayan, S.A.; Shafi, G.; Hasan, T.N.; Syed, N.A.; Alshatwi, A.A. Luminescent mesoporous lavo4:Eu3+ core-shell nanoparticles: Synthesis, characterization, biocompatibility and their cytotoxicity. *J Mater Chem* **2011**, *21*, 19310-19316.
30. Ansari, A.A.; Labis, J.P.; Manthrammel, M.A. Designing of luminescent gdpo4:Eu@lapo4@sio2 core/shell nanorods: Synthesis, structural and luminescence properties. *Solid State Sciences* **2017**, *71*, 117-122.
31. Slowing, I.I.; Trewyn, B.G.; Lin, V.S.Y. Mesoporous silica nanoparticles for intracellular delivery of membrane-impermeable proteins. *J Am Chem Soc* **2007**, *129*, 8845-8849.
32. Ansari, A.A.; Hasan, T.N.; Syed, N.A.; Labis, J.P.; Parchur, A.K.; Shafi, G.; Alshatwi, A.A. In-vitro cyto-toxicity, geno-toxicity, and bio-imaging evaluation of one-pot synthesized luminescent functionalized mesoporous sio2@eu(oh)(3) core-shell microspheres. *Nanomedicine-Nanotechnology Biology and Medicine* **2013**, *9*, 1328-1335.
33. Ansari, A.A.; Labis, J.P. One-pot synthesis and photoluminescence properties of luminescent functionalized mesoporous sio2@tb(oh)(3) core-shell nanospheres. *J Mater Chem* **2012**, *22*, 16649-16656.
34. Radu, D.R.; Lai, C.Y.; Jeftinija, K.; Rowe, E.W.; Jeftinija, S.; Lin, V.S.Y. A polyamidoamine dendrimer-capped mesoporous silica nanosphere-based gene transfection reagent. *J Am Chem Soc* **2004**, *126*, 13216-13217.
35. Luo, Z.; Cai, K.Y.; Hu, Y.; Zhao, L.; Liu, P.; Duan, L.; Yang, W.H. Mesoporous silica nanoparticles end-capped with collagen: Redox-responsive nanoreservoirs for targeted drug delivery. *Angew Chem Int Edit* **2011**, *50*, 640-643.
36. Paek, J.; Lee, C.H.; Choi, J.; Choi, S.Y.; Kim, A.; Lee, J.W.; Lee, K. Gadolinium oxide nanoring and nanoplate: Anisotropic shape control. *Crystal Growth & Design* **2007**, *7*, 1378-1380.
37. Gaspar, R.D.L.; Mazali, I.O.; Sigoli, F.A. Particle size tailoring and luminescence of europium(iii)-doped gadolinium oxide obtained by the modified homogeneous precipitation method: Dielectric constant and counter anion effects. *Colloids and Surfaces a-Physicochemical and Engineering Aspects* **2010**, *367*, 155-160.
38. Guo, H.C.; Idris, N.M.; Zhang, Y. Lret-based biodetection of DNA release in live cells using surface-modified upconverting fluorescent nanoparticles. *Langmuir* **2011**, *27*, 2854-2860.
39. Wang, Y.; Yang, T.; Ke, H.T.; Zhu, A.J.; Wang, Y.Y.; Wang, J.X.; Shen, J.K.; Liu, G.; Chen, C.Y.; Zhao, Y.L*., et al.* Smart albumin-biomineralized nanocomposites for multimodal imaging and photothermal tumor ablation. *Adv Mater* **2015**, *27*, 3874-+.
40. Park, J.Y.; Baek, M.J.; Choi, E.S.; Woo, S.; Kim, J.H.; Kim, T.J.; Jung, J.C.; Chae, K.S.; Chang, Y.; Lee, G.H. Paramagnetic ultrasmall gadolinium oxide nanoparticles as advanced t-1 mr1 contrast agent: Account for large longitudinal relaxivity, optimal particle diameter, and in vivo t-1 mr images. *Acs Nano* **2009**, *3*, 3663-3669.
41. Paul, N.; Mohanta, D. Evaluation of optoelectronic response and raman active modes in tb3+ and eu3+-doped gadolinium oxide (gd2o3) nanoparticle systems. *Appl Phys a-Mater* **2016**, *122*.
42. Runowski, M.; Goderski, S.; Paczesny, J.; Ksiezopolska-Gocalska, M.; Ekner-Grzyb, A.; Grzyb, T.; Rybka, J.D.; Giersig, M.; Lis, S. Preparation of biocompatible, luminescent-

plasmonic core/shell nanomaterials based on lanthanide and gold nanoparticles exhibiting sers effects. *J Phys Chem C* **2016**, *120*, 23788-23798.

43. Grzyb, T.; Runowski, M.; Dąbrowska, K.; Giersig, M.; Lis, S. Structural, spectroscopic and cytotoxicity studies of tbf3@cef3 and tbf3@cef3@sio2 nanocrystals. *J Nanopart Res* **2013**, *15*, 1-15.
44. Runowski, M.; Grzyb, T.; Zep, A.; Krzyczkowska, P.; Gorecka, E.; Giersig, M.; Lis, S. Eu3+ and tb3+ doped lapo4 nanorods, modified with a luminescent organic compound, exhibiting tunable multicolour emission. *Rsc Adv* **2014**, *4*, 46305-46312.
45. Huang, C.C.; Su, C.H.; Li, W.M.; Liu, T.Y.; Chen, J.H.; Yeh, C.S. Bifunctional gd2o3/c nanoshells for mr imaging and nir therapeutic applications. *Advanced Functional Materials* **2009**, *19*, 249-258.
46. Li, Z.Q.; Wang, L.M.; Wang, Z.Y.; Liu, X.H.; Xiong, Y.J. Modification of nayf4:Yb,er@sio2 nanoparticles with gold nanocrystals for tunable green-to-red upconversion emissions. *J Phys Chem C* **2011**, *115*, 3291-3296.
47. Ansari, A.A.; Aldalbahi, A.K.; Labis, J.P.; Manthrammel, M.A. Impact of surface coating on physical properties of europium-doped gadolinium fluoride microspheres. *J Fluorine Chem* **2017**, *199*, 7-13.
48. Xu, Z.H.; Li, C.X.; Ma, P.A.; Hou, Z.Y.; Yang, D.M.; Kang, X.J.; Lin, J. Facile synthesis of an up-conversion luminescent and mesoporous gd2o3:Er3+@nsio(2)@msio(2) nanocomposite as a drug carrier. *Nanoscale* **2011**, *3*, 661-667.
49. Szczeszak, A.; Ekner-Grzyb, A.; Runowski, M.; Szutkowski, K.; Mrowczynska, L.; Kazmierczak, Z.; Grzyb, T.; Dabrowska, K.; Giersig, M.; Lis, S. Spectroscopic, structural and in vitro cytotoxicity evaluation of luminescent, lanthanide doped core@shell nanomaterials gdvo4:Eu(3+)5%@sio2@nh2. *J Colloid Interf Sci* **2016**, *481*, 245-255.
50. Grzyb, T.; Runowski, M.; Dabrowska, K.; Giersig, M.; Lis, S. Structural, spectroscopic and cytotoxicity studies of tbf3@cef3 and tbf3@cef3@sio2 nanocrystals. *Journal of Nanoparticle Research* **2013**, *15*.
51. Ansari, A.A.; Yadav, R.; Rai, S.B. Enhanced luminescence efficiency of aqueous dispersible nayf4:Yb/er nanoparticles and the effect of surface coating. *Rsc Adv* **2016**, *6*, 22074-22082.
52. Ansari, A.A.; Parchur, A.K.; Kumar, B.; Rai, S.B. Influence of shell formation on morphological structure, optical and emission intensity on aqueous dispersible nayf4:Ce/tb nanoparticles. *J Fluoresc* **2016**, *26*, 1151-1159.
53. Ansari, A.A.; Manthrammel, M.A. Surface coating effect on structural, optical and photoluminescence properties of eu3+ doped yttrium fluoride nanoparticles. *Journal of Inorganic and Organometallic Polymers and Materials* **2017**, *27*, 194-200.
54. Lechevallier, S.; Lecante, P.; Mauricot, R.; Dexpert, H.; Dexpert-Ghys, J.; Kong, H.K.; Law, G.L.; Wong, K.L. Gadolinium-europium carbonate particles: Controlled precipitation for luminescent biolabeling. *Chem Mater* **2010**, *22*, 6153-6161.
55. Ren, H.; Zhang, L.Y.; Wang, T.T.; Li, L.; Su, Z.M.; Wang, C.G. Universal and facile synthesis of multicolored upconversion hollow nanospheres using novel poly(acrylic acid sodium salt) microspheres as templates. *Chemical Communications* **2013**, *49*, 6036-6038.
56. Kang, J.G.; Min, B.K.; Sohn, Y. Synthesis and characterization of gd(oh)(3) and gd2o3 nanorods. *Ceram Int* **2015**, *41*, 1243-1248.
57. Li, J.G.; Zhu, Q.; Li, X.D.; Sun, X.D.; Sakka, Y. Colloidal processing of gd2o3:Eu3+ red phosphor monospheres of tunable sizes: Solvent effects on precipitation kinetics and photoluminescence properties of the oxides. *Acta Materialia* **2011**, *59*, 3688-3696.

58. Macedo, A.G.; Ferreira, R.A.S.; Ananias, D.; Reis, M.S.; Amaral, V.S.; Carlos, L.D.; Rocha, J. Effects of phonon confinement on anomalous thermalization, energy transfer, and upconversion in ln(3+)-doped gd2o3 nanotubes. *Advanced Functional Materials* **2010**, *20*, 624-634.
59. Xu, Z.H.; Gao, Y.; Huang, S.S.; Ma, P.A.; Lin, J.; Fang, J.Y. A luminescent and mesoporous core-shell structured gd2o3:Eu3+@nsio(2)@msio(2) nanocomposite as a drug carrier. *Dalton T* **2011**, *40*, 4846-4854.
60. Ansari, A.A.; Labis, J.P. Preparation and photoluminescence properties of hydrothermally synthesized yvo4:Eu3+ nanofibers. *Materials Letters* **2012**, *88*, 152-155.
61. Ansari, A.A.; Labis, J.P.; Alrokayan, S.A.H. Synthesis of water-soluble luminescent lavo4:Ln(3+) porous nanoparticles. *Journal of Nanoparticle Research* **2012**, *14*.
62. Goglio, G.; Kaur, G.; Pinho, S.L.C.; Penin, N.; Blandino, A.; Geraldes, C.F.G.C.; Garcia, A.; Delville, M.H. Glycine-nitrate process for the elaboration of eu3+-doped gd2o3 bimodal nanoparticles for biomedical applications. *European Journal of Inorganic Chemistry* **2015**, 1243-1253.
63. Guo, K.M.; Li, M.Y.; Fang, X.L.; Luoshan, M.D.; Bai, L.H.; Zhao, X.Z. Performance enhancement in dye-sensitized solar cells by utilization of a bifunctional layer consisting of core shell beta-nayf4:Er3+/yb3+@sio2 submicron hexagonal prisms. *Journal of Power Sources* **2014**, *249*, 72-78.
64. He, E.J.; Zheng, H.R.; Dong, J.; Gao, W.; Han, Q.Y.; Li, J.N.; Hui, L.; Lu, Y.; Tian, H.N. Facile fabrication and upconversion luminescence enhancement of laf3:Yb3+/ln(3+)@sio2 (ln = er, tm) nanostructures decorated with ag nanoparticles. *Nanotechnology* **2014**, *25*.
65. Kang, X.J.; Cheng, Z.Y.; Li, C.X.; Yang, D.M.; Shang, M.M.; Ma, P.A.; Li, G.G.; Liu, N.A.; Lin, J. Core-shell structured up-conversion luminescent and mesoporous nayf4:Yb3+/er3+@nsio(2)@msio(2) nanospheres as carriers for drug delivery. *Journal of Physical Chemistry C* **2011**, *115*, 15801-15811.
66. Kostiv, U.; Patsula, V.; Noculak, A.; Podhorodecki, A.; Vetvicka, D.; Pouckova, P.; Sedlakova, Z.; Horak, D. Phthalocyanine-conjugated upconversion nayf4:Yb3+/er3+@sio2 nanospheres for nir-triggered photodynamic therapy in a tumor mouse model. *Chemmedchem* **2017**, *12*, 2066-2073.
67. Jacobsohn, L.G.; Bennett, B.L.; Muenchausen, R.E.; Tornga, S.C.; Thompson, J.D.; Ugurlu, O.; Cooke, D.W.; Sharma, A.L.L. Multifunction gd2o3 : Eu nanocrystals produced by solution combustion synthesis: Structural, luminescent, and magnetic characterization. *Journal of Applied Physics* **2008**, *103*.
68. Ansari, A.A.; Parchur, A.K.; Kumar, B.; Rai, S.B. Highly aqueous soluble caf2:Ce/tb nanocrystals: Effect of surface functionalization on structural, optical band gap, and photoluminescence properties. *Journal of Materials Science-Materials in Medicine* **2016**, *27*.
69. Shi, F.; Zhai, X.S.; Zheng, K.Z.; Zhao, D.; Qin, W.P. Synthesis of monodisperse nayf4:Yb, tm@sio2 nanoparticles with intense ultraviolet upconversion luminescence. *Journal of Nanoscience and Nanotechnology* **2011**, *11*, 9912-9915.
70. Sotiriou, G.A.; Franco, D.; Poulikakos, D.; Ferrari, A. Optically stable biocompatible flame-made sio2-coated y2o3: Tb3+ nanophosphors for cell imaging. *Acs Nano* **2012**, *6*, 3888-3897.

 doi:10.20944/preprints201809.0138.v1

Figure Captions

Fig.1. X-ray diffraction pattern of Core, Core/nSiO_2 and Core/nSiO_2/mSiO_2 NPs.
Fig.2. TEM images of (a&b) core (c) high resolution core image (d) low resolution core/nSiO_2/mSiO_2 image (e) high magnification core/nSiO_2/mSiO_2 image (f) EDX spectrum of core and (g) EDX spectrum of core/nSiO_2/mSiO_2 NPs.
Fig.3. Zeta-potential graphs of (a) core (b) core/nSiO_2 and (c) core/nSiO_2/mSiO_2 NPs.
Fig.4. Thermo-gravimetric analysis of Core and Core/nSiO_2 NPs.
Fig.5. UV-vis absorption spectra of Core and Core/nSiO_2 NPs suspended in de-ionized water.
Fig.6. FTIR spectra of the as-prepared Core, Core/nSiO_2 and Core/nSiO_2/mSiO_2 NPs.
Fig.7. Excitation spectra of the as-prepared Core, Core/nSiO_2 and Core/nSiO_2/mSiO_2 NPs.
Fig.8. Emission spectra of the as-prepared Core, Core/nSiO_2 and Core/nSiO_2/mSiO_2 NPs.

Preprints (www.preprints.org) | NOT PEER-REVIEWED | Posted: 7 September 2018 doi:10.20944/preprints201809.0138.v1

Figure.1.

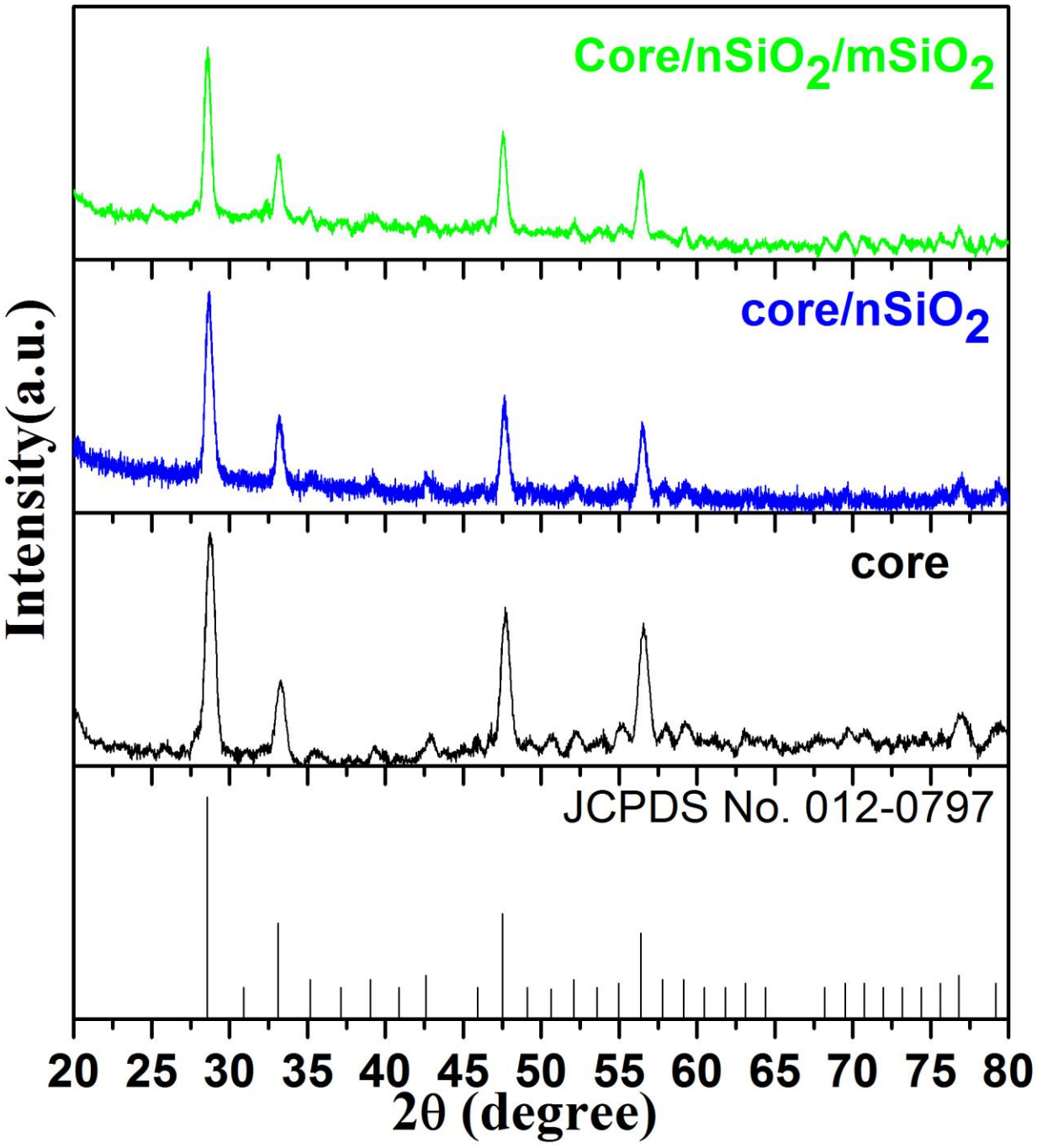

Preprints (www.preprints.org) | NOT PEER-REVIEWED | Posted: 7 September 2018 doi:10.20944/preprints201809.0138.v1

Figure.2

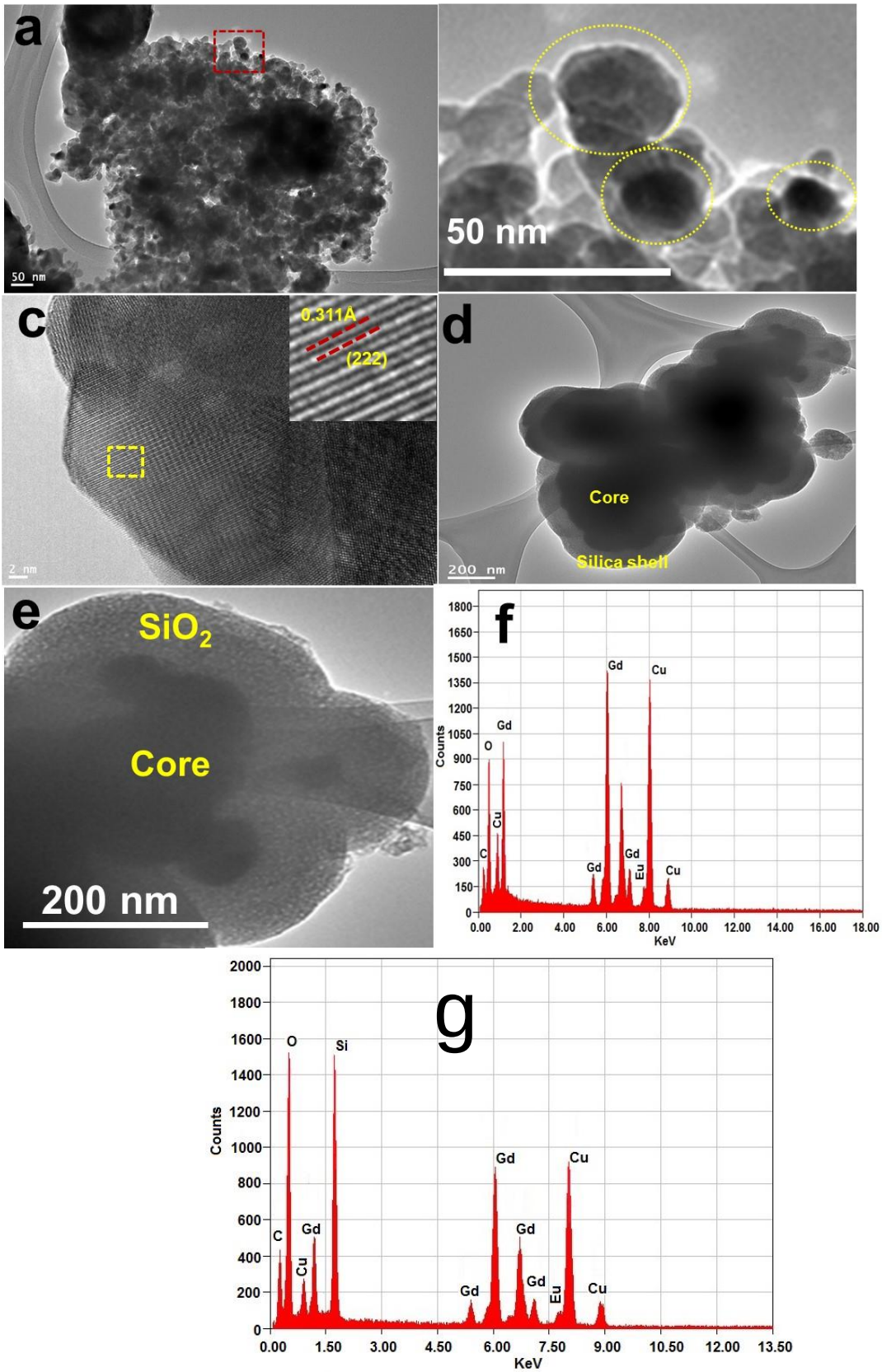

Preprints (www.preprints.org) | NOT PEER-REVIEWED | Posted: 7 September 2018 doi:10.20944/preprints201809.0138.v1

Figure.3

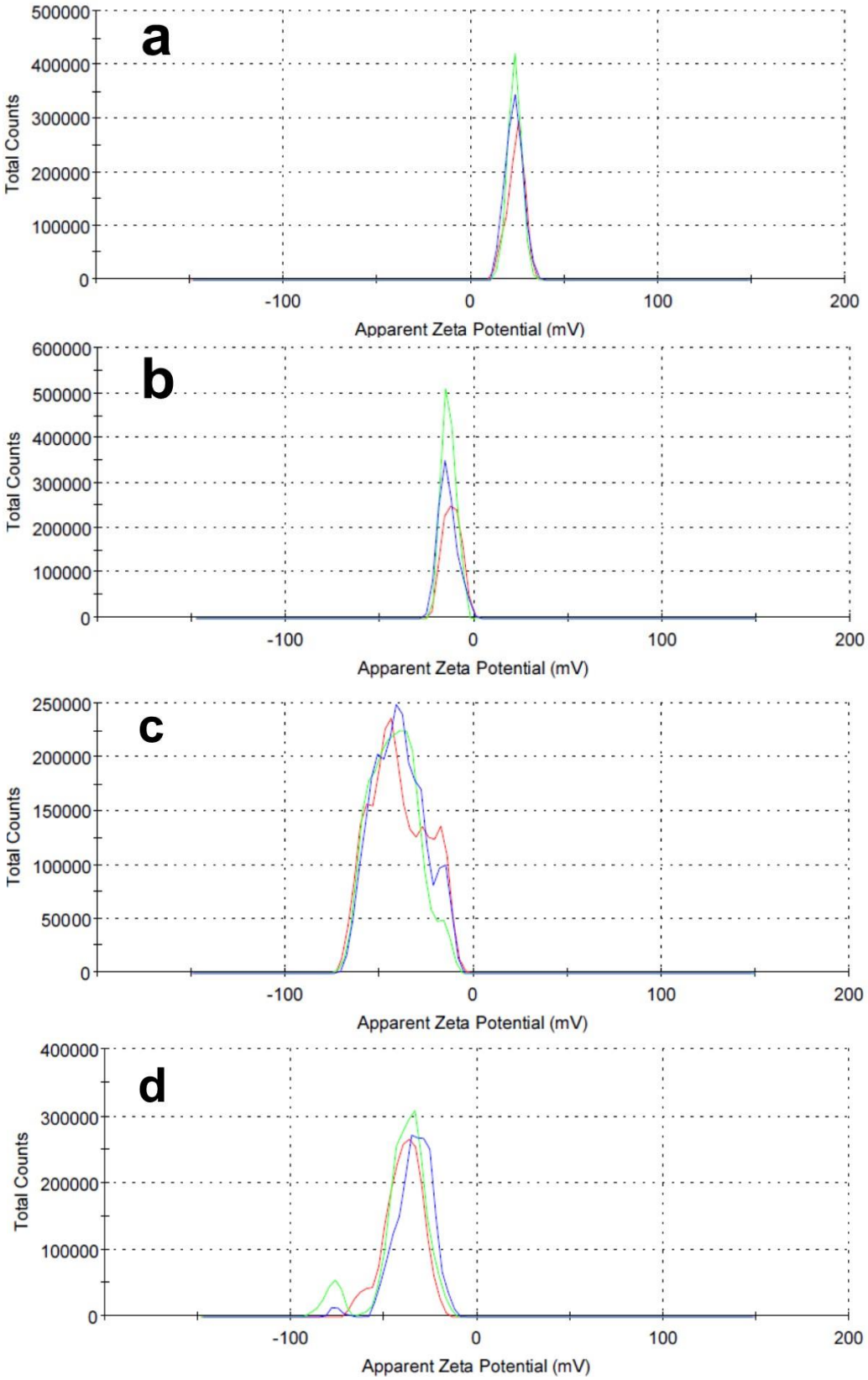

Preprints (www.preprints.org) | NOT PEER-REVIEWED | Posted: 7 September 2018 doi:10.20944/preprints201809.0138.v1

Figure 4

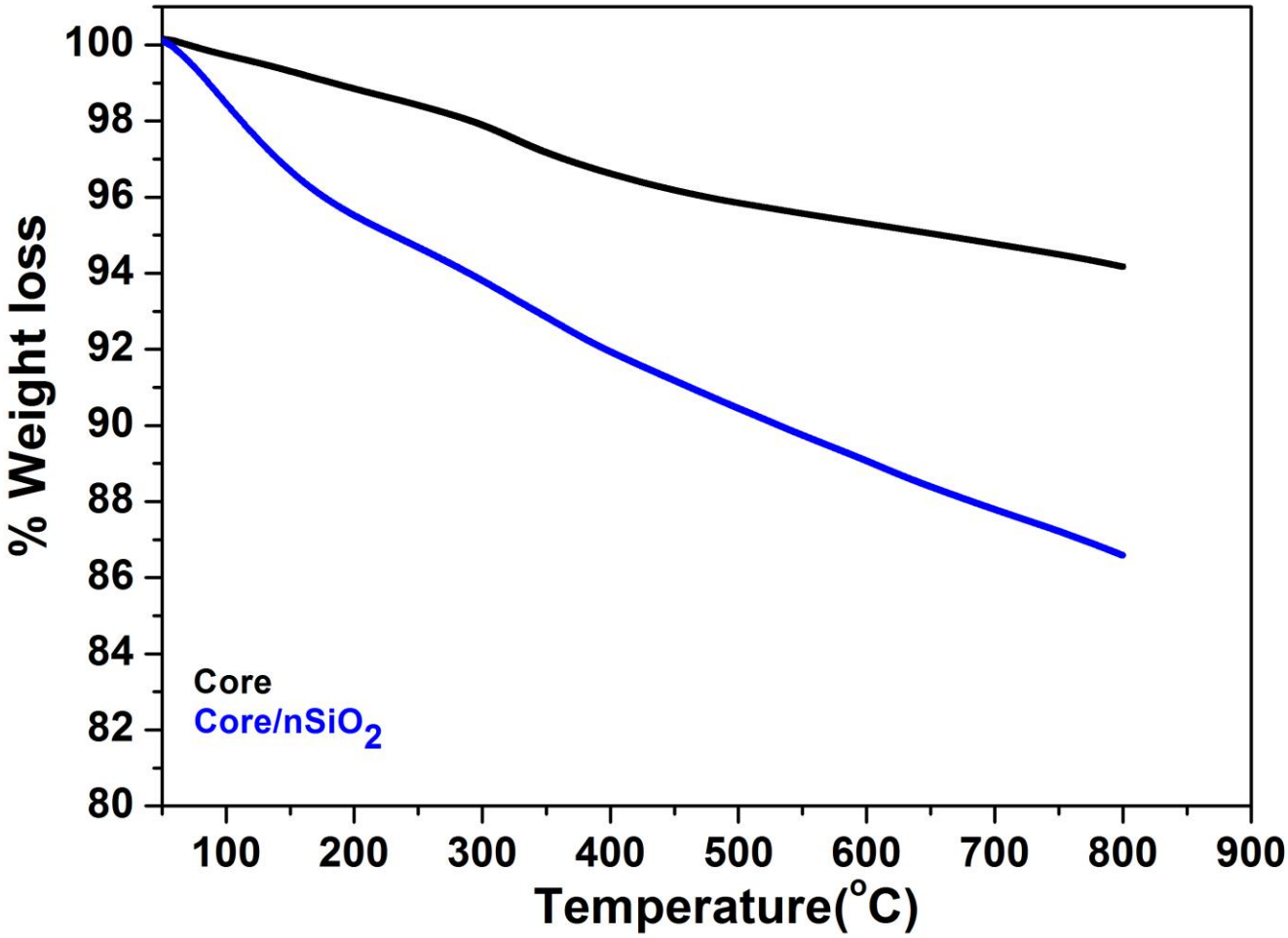

Preprints (www.preprints.org) | NOT PEER-REVIEWED | Posted: 7 September 2018 doi:10.20944/preprints201809.0138.v1

Figure 5

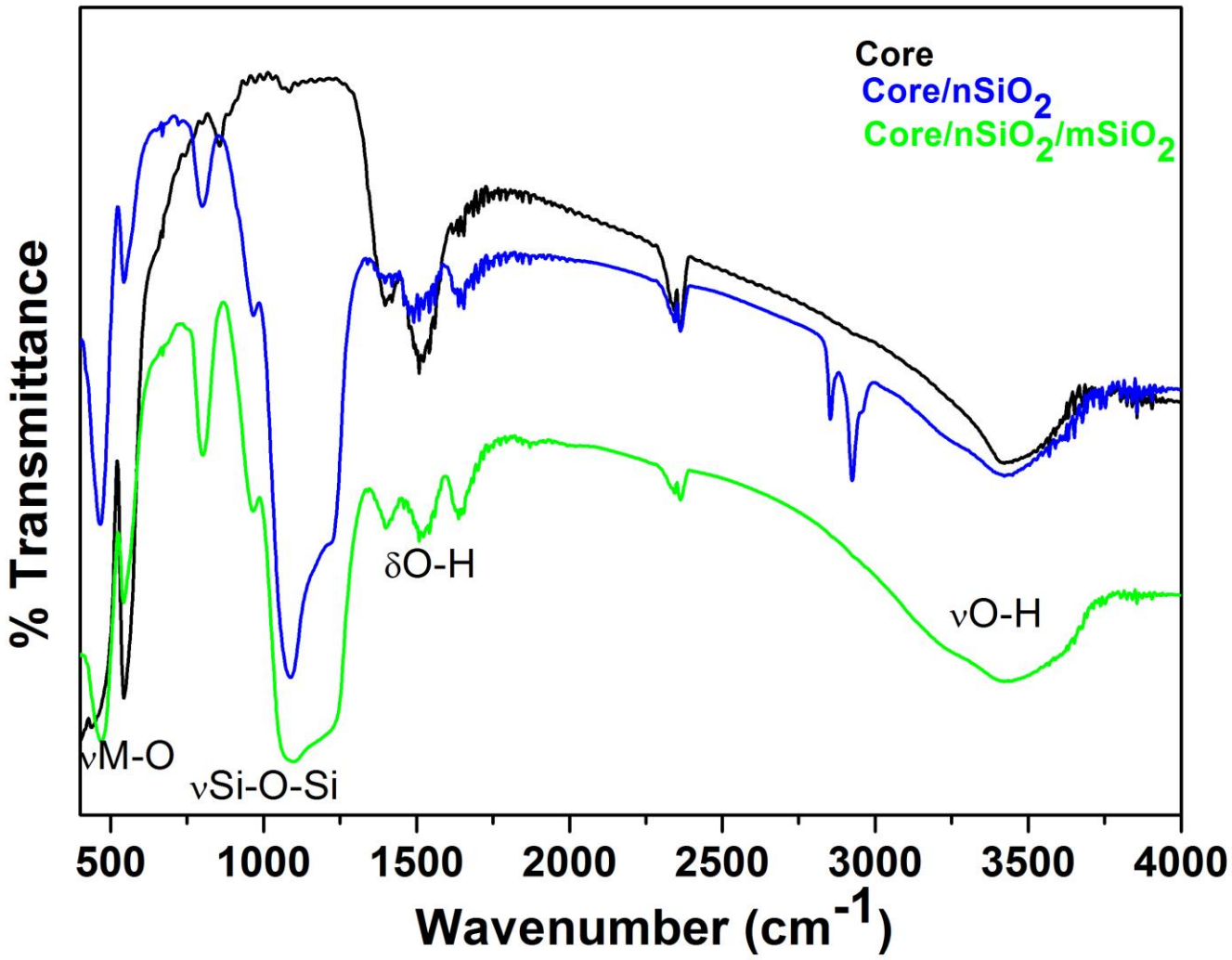

Preprints (www.preprints.org) | NOT PEER-REVIEWED | Posted: 7 September 2018 doi:10.20944/preprints201809.0138.v1

Figure 6

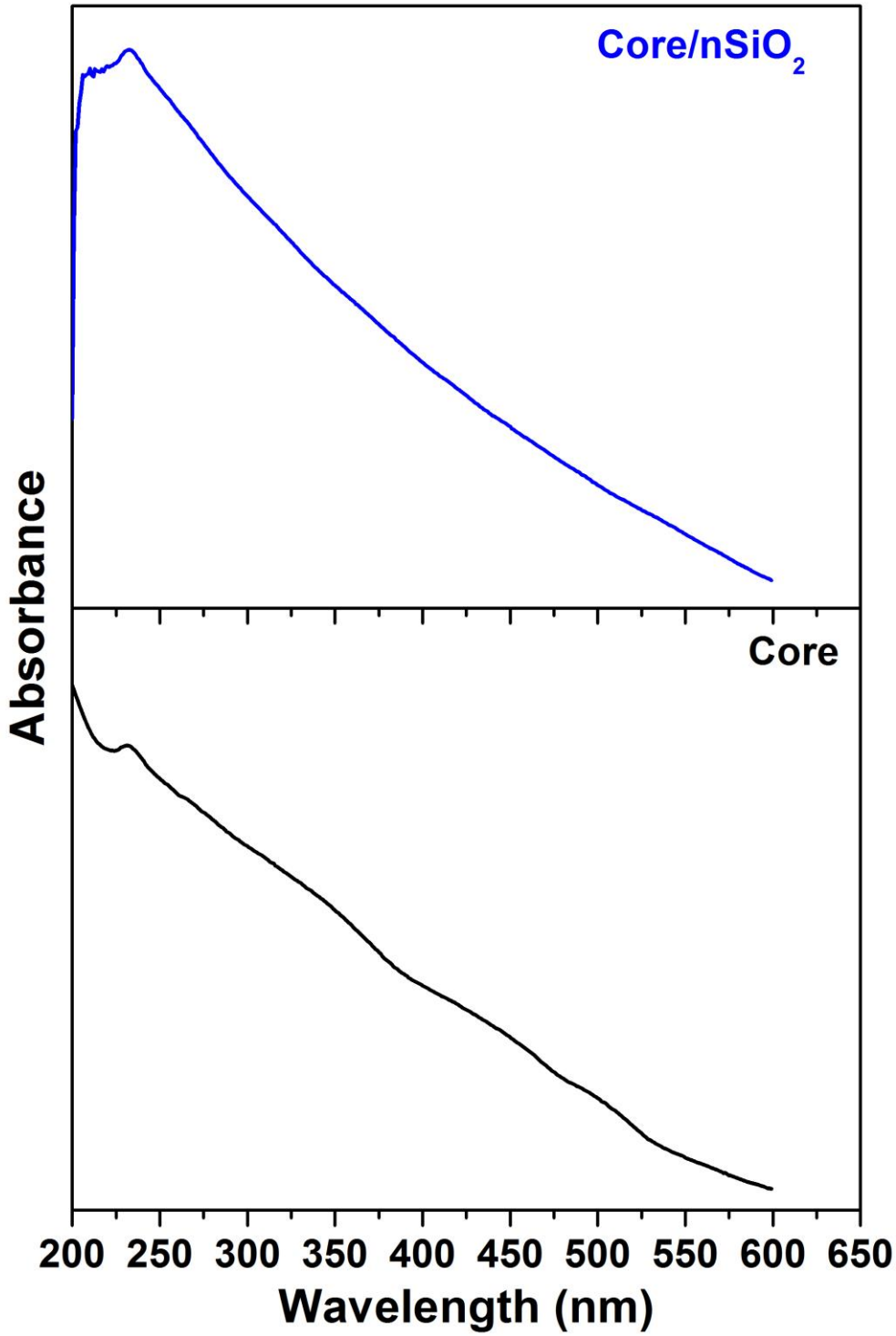

Preprints (www.preprints.org) | NOT PEER-REVIEWED | Posted: 7 September 2018 doi:10.20944/preprints201809.0138.v1

Figure 7

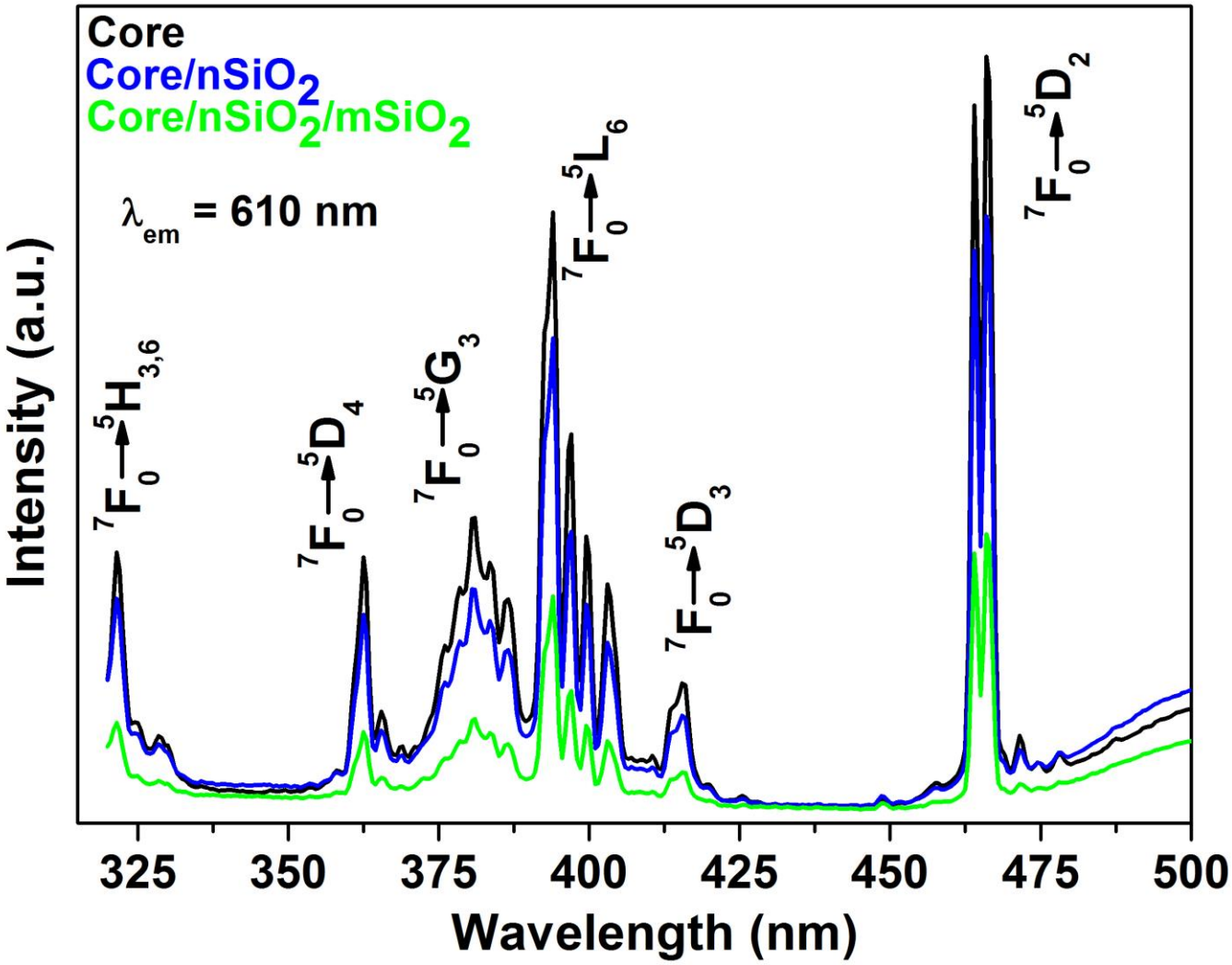

Preprints (www.preprints.org) | NOT PEER-REVIEWED | Posted: 7 September 2018 doi:10.20944/preprints201809.0138.v1

Figure 8